

EDN: Salient Object Detection via Extremely-Downsampled Network

Yu-Huan Wu^{1*} Yun Liu^{1*} Le Zhang² Ming-Ming Cheng^{1†}
¹TKLNDST, College of Computer Science, Nankai University ²A*STAR

Abstract

Recent progress on salient object detection (SOD) mainly benefits from multi-scale learning, where the high-level and low-level features work collaboratively in locating salient objects and discovering fine details, respectively. However, most efforts are devoted to low-level feature learning by fusing multi-scale features or enhancing boundary representations. In this paper, we show another direction that improving high-level feature learning is essential for SOD as well. To verify this, we introduce an Extremely-Downsampled Network (EDN), which employs an extreme downsampling technique to effectively learn a global view of the whole image, leading to accurate salient object localization. A novel Scale-Correlated Pyramid Convolution (SCPC) is also designed to build an elegant decoder for recovering object details from the above extreme downsampling. Extensive experiments demonstrate that EDN achieves state-of-the-art performance with real-time speed. Hence, this work is expected to spark some new thinking in SOD. The code will be released.

1. Introduction

Salient object detection (SOD), also called saliency detection, tries to simulate the human visual system to detect the most salient and eye-catching objects or regions in natural images [4, 14]. It has been demonstrated to be useful for far-reaching computer vision applications such as visual tracking [27], scene classification [33], image retrieval [6], and weakly supervised learning [25]. Although much progress has been made recently [2, 9, 12, 19, 24, 30, 62], it is still challenging to detect complete salient objects in complicated scenarios accurately.

In the last several years, convolutional neural networks (CNNs) have achieved vast successes in this field [16, 17, 23, 26, 42, 54]. These networks usually employ *multi-scale learning* to leverage both high-level semantic features and fine-grained low-level representations, in which the former is effective in accurately locating salient objects and the lat-

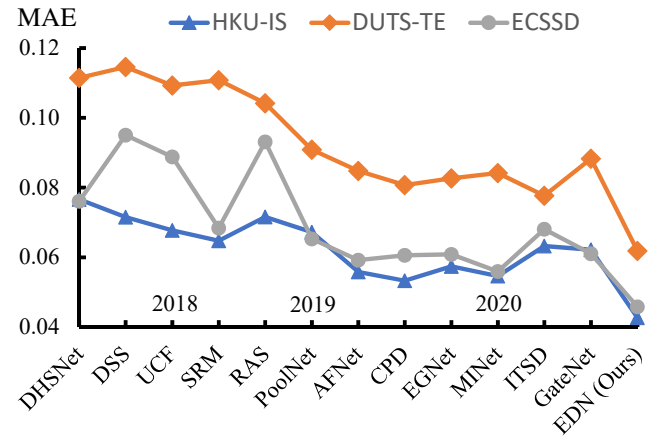


Figure 1. MAE of various SOD methods for the center of salient objects. This measures the capability of a method for locating salient objects. Please refer to §4 for detailed experimental settings. From left to right, various methods are sorted by the publication date. It is clear to see that the accuracy for salient object localization has been saturated since 2019.

ter works better in discovering object details and boundaries. In addition, such a multi-scale learning is a natural solution to tackle the large scale variations in practice. Hence, most recent efforts for saliency detection are devoted to designing advanced network architectures to facilitate multi-scale learning [2, 10, 24, 40–42, 52, 54, 55].

Existing multi-scale learning methods in SOD mainly aim at dealing with *low-level feature learning* for better capturing/utilizing fine-grained object details/boundaries explicitly or implicitly. For exploring fine-grained details explicitly, recent works [5, 19, 22, 32, 37, 43, 45, 46, 48, 59, 63] try to improve the accuracy of salient object boundaries by enhancing boundary representations and imposing boundary supervision to predictions directly. For exploring fine-grained details implicitly, many studies [2, 9, 12, 13, 21, 24, 40, 42, 54, 55] design various multi-level feature fusion strategies to serve high-level semantics with low-level fine details, for example, the hot U-Net [34] or so-called encoder-decoder based saliency detectors [9, 12, 13, 21, 23, 24, 42, 55]. Although workable as reported, recent SOD has reached a bottleneck period as many existing methods can handle object boundaries very well.

*Equal contributions. Author ordering determined by a coin flip.

†M.M. Cheng is the corresponding author (cmm@nankai.edu.cn).

To break through this bottleneck of SOD, an intuitive idea is to investigate the other aspect of multi-scale learning, *i.e.*, *high-level feature learning*, which plays an essential role in scene understanding and further locating salient objects. Unfortunately, this direction is less investigated. For better high-level feature learning, existing SOD methods [22, 40, 53, 54, 61] usually directly apply some well-known modules developed for semantic segmentation, such as ASPP [1] and PSP modules [57]. However, SOD requires different high-level feature learning from semantic segmentation. Specifically, semantic segmentation requires learning the relationship between each pixel and all other pixels so that we can make accurate prediction according to such relationship. As a result, semantic segmentation methods usually aims at enlarging the receptive field to extract large-scale features for each pixel [1, 11, 57, 64]. On the other hand, salient object detection requires locating salient objects, which is an overall understanding of an image. With salient object locations, object details can be easily recovered using a decoder, like previous SOD methods that focus on low-level feature learning. As shown in Fig. 1, the accuracy for locating salient objects has been saturated recently due to the limitation of high-level feature learning. In a word, semantic segmentation needs to learn the global relationship for each pixel, while SOD needs to learn *a global view of the whole image*. Therefore, directly applying semantic segmentation methods to SOD can only achieve sub-optimal performance.

To this end, this paper aims to enhance high-level feature learning, which is expected to open a new path for future development of SOD. We propose an **Extremely-Downsampled Block (EDB)** to learn a global view of the whole image. EDB gradually downsamples the feature map until it becomes a feature vector, *i.e.*, with the size of 1×1 . In such a downsampling process, we continue learning deep features. With the feature map becomes smaller, the learned feature becomes more global. Until downsampling to a feature vector, we obtain a global view of the whole image so that we can locate salient objects accurately. Note that EDB only introduces a little extra computational cost, as it operates on a very low feature resolution. To recover complete salient objects from the global view, we build an elegant decoder to aggregate multi-level features from top to bottom gradually. For this goal, we design a **Scale-Correlated Pyramid Convolution (SCPC)** for effective feature fusion in the decoder. Unlike traditional methods (*e.g.*, ASPP [1] and PSP [57]) that only adopt multiple parallel branches to extract multi-scale features *separately*, SCPC adds *correlation* among various branches/scales. With EDB and SCPC incorporated, the proposed **Extremely-Downsampled Network (EDN)** achieves state-of-the-art performance on five challenging benchmarks with fast speed and a small number of parameters.

To summarize, our contributions are as below:

- We propose to explore high-level feature learning for locating salient objects instead of previous low-level feature utilization for improving object boundaries, which is expected to open a new path for SOD.
- We propose an intuitive extreme downsampling technique for learning a global view of the whole image, which generates effective high-level features for salient object localization.
- We design an SCPC for effective multi-level feature fusion, which adds correlation among various feature scales and serves as the basic unit of an elegant decoder for accurate SOD.

2. Related Work

SOD is a fundamental problem in computer vision and thus there are a plethora of studies in the literature.

Initiated SOD methods. The initiated works utilize hand-crafted features, and many shallow learning methods have been developed [7, 38, 49]. Apart from these approaches, heuristic saliency priors also see heavy usage in this domain. Examples include but are not limited to color contrast [4], center prior [14], background prior [51], and so on. However, those types of methods are lacking, especially compared with more recently-proposed methods, largely due to its limited representational capability.

CNN-based SOD methods. Inspired by the vast successes achieved by deep CNNs in other computer vision tasks, CNN-based methods have become the dominant methods for SOD. Early CNN-based methods process and classify image regions for saliency prediction [16, 18, 60], which discards the spatial layout of the input image. Motivated by the superiority of fully convolutional network (FCN) [35], later attention has been shifted toward end-to-end image-to-image SOD [2, 10, 52, 54, 55, 58]. As widely acknowledged that high-level semantic features in the top CNN layers are effective in accurately locating salient objects and low-level fine-grained features in the bottom CNN layers work better in discovering object details, most of the recent efforts are devoted to designing effective networks to facilitate multi-scale learning.

Multi-level feature fusion. Most CNN-based SOD methods achieve multi-scale learning by designing advanced network architectures for multi-level feature fusion, so that the final fused features contain both high-level semantics and low-level fine details. The architectures of these methods are usually based on HED [2, 10], Hypercolumns [37, 40, 52, 61], or the typical U-Net [9, 12, 13, 21, 23, 24, 42, 55]. Their target is to add low-level fine-grained

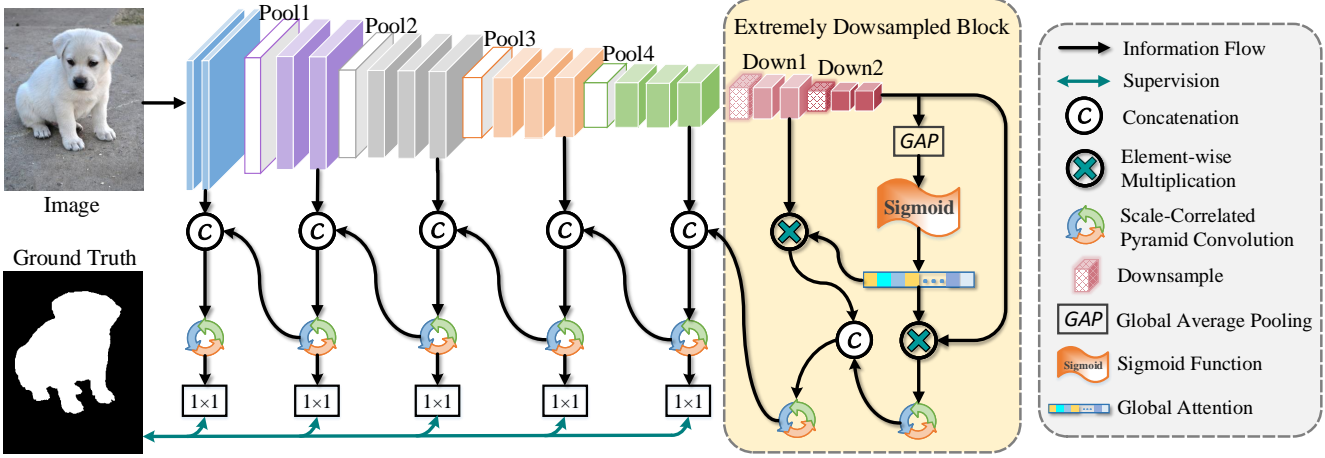


Figure 2. Illustration of the overall network architecture of EDN. We stack EDB on top of the backbone network to learn a global view of the whole image for more accurate salient object localization. SCPC is designed as well for effective multi-level feature integration in the decoder. Each downsampling operation downsamples the feature map by half except GAP.

features into the fused features without weakening the representation capability of high-level features, segmenting the located salient objects with clear boundaries.

Boundary-aware SOD methods. Besides the above multi-level feature fusion, the recent SOD trend directly uses boundary information to improve the SOD accuracy at object boundaries [2, 9, 12, 13, 21, 24, 40, 42, 54, 55]. For example, Zhao *et al.* [59] applied boundary supervision to low-level features. Liu *et al.* [22] conducted joint supervision of salient objects and object boundaries at each side-output. Zhou *et al.* [63] designed a two-stream network that uses two branches to learn the boundary details and locations of salient objects, respectively.

High-level feature learning. While tremendous progress has been achieved, existing SOD methods mainly explore the fusion or enhancement of low-level features to better discover object boundaries, leading high-level feature learning less investigated. To strengthen the high-level features, these methods [22, 40, 53, 54, 61] usually adopt some well-known modules developed for semantic segmentation, such as ASPP [1], PSP [57], or their variants. Due to the natural difference between SOD and semantic segmentation, as discussed above, current SOD methods can only achieve suboptimal accuracy in locating salient objects. In this paper, we contribute from this aspect by proposing an extreme downsampling technique for better learning high-level representation in SOD.

3. Methodology

In this section, we first provide an overview of our method in §3.1. Then, we introduce an extreme downsampling technique in §3.2. At last, we present the proposed SCPC in §3.3.

3.1. Overview

The overall structure of the proposed EDN is illustrated in Fig. 2. Without loss of generality, we take VGG16 [36] as an example backbone network to introduce EDN. We follow previous studies [12, 13, 21, 24, 24, 42] to remove the last pooling layers and all fully connected layers, resulting in an FCN [35] for image-to-image saliency prediction. So far VGG16 has 13 convolutional layers, separated by four pooling layers. Hence, our encoder has five convolution stages, whose outputs are denoted as E_1, E_2, E_3, E_4 , and E_5 , with scales of $1, \frac{1}{2}, \frac{1}{4}, \frac{1}{8}$, and $\frac{1}{16}$, respectively.

As discussed above, we propose an EDB to learn a global view of the whole image so that we can locate salient objects accurately. Suppose \mathcal{F} denotes the function of EDB. We stack EDB on top of VGG16, and the output can be written as

$$D_6 = \mathcal{F}(E_5), \quad (1)$$

in which D_6 has a scale of $\frac{1}{32}$. Here, we argue that extreme downsampling does great benefit to achieve SOD by learning a global view of the whole image. After EDB, we perform top-down multi-level feature integration with the proposed SCPC for predicting saliency maps with fine details. Let \mathcal{H} be the function of SCPC. Our decoder can be elegantly formulated as

$$\begin{aligned} D'_{i+1} &= \text{Upsample}(\text{Conv}_{1 \times 1}(D_{i+1})), \\ D_i &= \mathcal{H}(\text{Concat}(\text{Conv}_{1 \times 1}(E_i), D'_{i+1})), \end{aligned} \quad (2)$$

where we have $i \in \{1, 2, \dots, 5\}$. $\text{Conv}_{1 \times 1}(\cdot)$ represents a 1×1 convolution followed by batch normalization and ReLU layers. $\text{Upsample}(\cdot)$ upsamples its input feature map by a scale of 2. $\text{Concat}(\dots)$ concatenates the input feature maps along the channel dimension. In this way, we can

effectively fuse multi-level features in an elegant way and obtain decoder outputs D_1, D_2, D_3, D_4, D_5 , and D_6 .

We continue by introducing our loss function for optimizing the proposed EDN. Let \mathcal{L} stands for the combination of commonly-used binary cross-entropy loss \mathcal{L}_{bce} and Dice loss \mathcal{L}_{dice} [29], which can be defined as

$$\begin{aligned}\mathcal{L}_{bce}(P, G) &= G \log P + (1 - G) \log(1 - P), \\ \mathcal{L}_{dice}(P, G) &= 1 - \frac{2 \cdot G \cdot P}{\|G\| + \|P\|}, \\ \mathcal{L}(P, G) &= \mathcal{L}_{bce} + \mathcal{L}_{dice},\end{aligned}\quad (3)$$

where P and G denote the predicted and ground-truth saliency map, respectively. “.” operation indicates the dot product. $\|\cdot\|$ denotes the ℓ_1 norm. The Dice loss is known as an effective way to solve the class imbalance of foreground and background. The total loss for training EDN can be calculated as

$$\begin{aligned}P_i &= \sigma(\text{Upsample}(\text{Conv}_{1 \times 1}(D_i))), \\ L &= \sum_{i=1}^5 \mathcal{L}(P_i, G),\end{aligned}\quad (4)$$

in which $\text{Conv}_{1 \times 1}(\cdot)$ does not have batch normalization and ReLU activation. $\text{Upsample}(\cdot)$ upsamples the prediction into the size of the input image. $\sigma(\cdot)$ is the standard sigmoid function. We do not use D_6 in Equ. (4) due to its small size. During testing, P_1 is viewed as the final output prediction of EDN.

3.2. Extremely-Downsampled Block

In the above, we have discussed that existing SOD methods only focus on learning or utilizing low-level features, but ignore high-level feature learning. Hence, we propose EDB to strengthen high-level features by learning a global view of the whole image, which leads to more accurate salient object localization (as shown in Fig. 1). In this part, we clarify the design details of EDB.

Suppose that the input of an EDB is X . We first design a simple downsampling block to downsample the input feature map by a factor of 2 (“Down1” in Fig. 2). This can be formulated as

$$X_1 = \text{Conv}_{3 \times 3}(\text{Conv}_{3 \times 3}(\text{Downsample}(X))), \quad (5)$$

where $\text{Downsample}(\cdot)$ downsamples the input by a factor of 2. $\text{Conv}_{3 \times 3}(\cdot)$ is a 3×3 convolution with 256 output channels, followed by batch normalization and ReLU activation. We repeat this block to get X_2 (“Down2” in Fig. 2), like

$$X_2 = \text{Conv}_{3 \times 3}(\text{Conv}_{3 \times 3}(\text{Downsample}(X_1))). \quad (6)$$

X_2 is in a small scale and thus has a very large receptive field. To get a global view of the whole image, we further

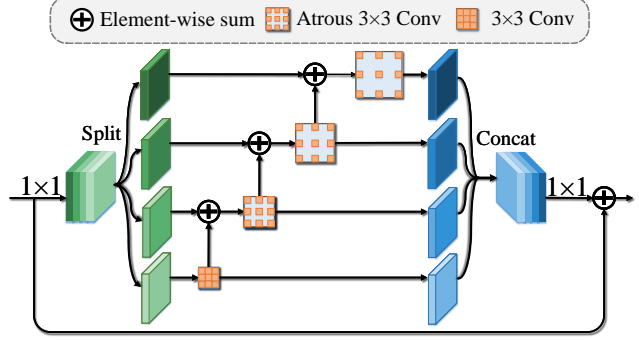


Figure 3. Illustration of SCPC for multi-scale learning.

downsample X_2 into a feature vector using global average pooling (GAP), which can be written as

$$X_3 = \sigma(\text{GAP}(X_2)). \quad (7)$$

The value range of X_3 is squeezed into $[0, 1]$ using a sigmoid function. Although X_3 is a global representation of the input image, its size of a single pixel makes it unsuitable to start decoding from it. Instead, we adopt it as a self-attention to recalibrate X_2 as

$$X'_2 = X_2 \otimes X_3, \quad (8)$$

in which \otimes represents element-wise multiplication and X_3 is replicated into the same size as X_2 before multiplication. We also adopt X_3 as a nonself-attention to recalibrate X_1 as

$$X'_1 = X_1 \otimes X_3. \quad (9)$$

In this way, X'_1 and X'_2 are enhanced by the global representation. Then, we fuse X'_1 and X'_2 , which can be formulated as

$$\begin{aligned}X''_2 &= \text{Upsample}(\text{Conv}_{1 \times 1}(\mathcal{H}(X'_2))), \\ Y &= \mathcal{H}(\text{Concat}(\text{Conv}_{1 \times 1}(X'_1), X''_2)),\end{aligned}\quad (10)$$

where Y is the output, *i.e.*, $Y = \mathcal{F}(X)$. Y is expected to be equipped with a global view of the whole image for better locating salient objects.

3.3. Scale-Correlated Pyramid Convolution

We propose SCPC for better fusing multi-level features, which is also an important aspect of multi-scale learning. Our motivation comes from that existing modules usually conduct *separate* multi-scale feature extraction. For example, ASPP [1], PSP [57], and their numerous variants use *separate* branches to extract multi-scale features, with different branches responsible for different feature scales. An intuitive idea is that the feature extraction at different scales should be correlated and benefit from each other. Suppose that M represents the input of SCPC. We first apply a 1×1 convolution for transition as

$$M_1 = \text{Conv}_{1 \times 1}(M). \quad (11)$$

Then, M_1 is split into four feature maps evenly along the channel dimension, *i.e.*,

$$M_2^1, M_2^2, M_2^3, M_2^4 = \text{Split}(M_1). \quad (12)$$

Next, we conduct multi-scale learning in a scale-correlated way, which can be formulated as

$$\begin{aligned} M_3^1 &= \text{Conv}_{3 \times 3}^{a_1}(M_2^1), \\ M_3^i &= \text{Conv}_{3 \times 3}^{a_i}(M_2^i + M_3^{i-1}), \quad i \in \{2, 3, 4\}, \end{aligned} \quad (13)$$

in which $\text{Conv}_{3 \times 3}^{a_i}(\cdot)$ is a 3×3 atrous convolution with an atrous rate of a_i . At last, we concatenate multi-scale features and add a residual connection, like

$$O = \text{Conv}_{1 \times 1}(\text{Concat}(M_3^1, M_3^2, M_3^3, M_3^4)) + M, \quad (14)$$

where O is the output, *i.e.*, $O = \mathcal{H}(M)$. All convolutions in SCPC are followed by batch normalization and ReLU activation, except that Equ. (14) puts the ReLU of 1×1 convolution after the residual sum with M , as commonly used [8]. In this way, SCPC learns scale-correlated features effectively using small-scale features (with small atrous rates) to fill the holes of large-scale features (with large atrous rates) gradually through Equ. (13).

4. Effect of Extreme Downsampling

Before experiments, we first discuss the effect of the proposed extreme downsampling technique. In the above, we have clarified that existing SOD methods mainly focus on learning or better utilizing low-level fined-grained features to facilitate multi-scale learning. However, this paper explores another direction of multi-scale learning by enhancing high-level feature learning, *i.e.*, learning a global view of the whole image. Here, we statistically show the benefits from extreme downsampling. To this end, we divide the foreground of the ground-truth saliency map into boundaries, center regions, and other regions. Boundaries are foreground pixels whose Euclidean distance to the nearest background pixel is smaller than 5 pixels, while center regions cover foreground pixels whose Euclidean distance to the nearest background pixel is in the top 20%. Other regions refer to foreground regions other than boundaries and center regions. Some visualization examples of such division are displayed in the 3rd column of Fig. 4.

With the above definition, we compute mean absolute error (MAE) for center, boundary, and other regions, respectively. Please see §5.1 for more details about the metric and datasets. Note that when we compute MAE for one type of regions, the other two types of regions are ignored. The statistical results are shown in Tab. 1. We remove EDB from the proposed EDN to serve as the baseline. The relative improvement in Tab. 1 is the fraction of

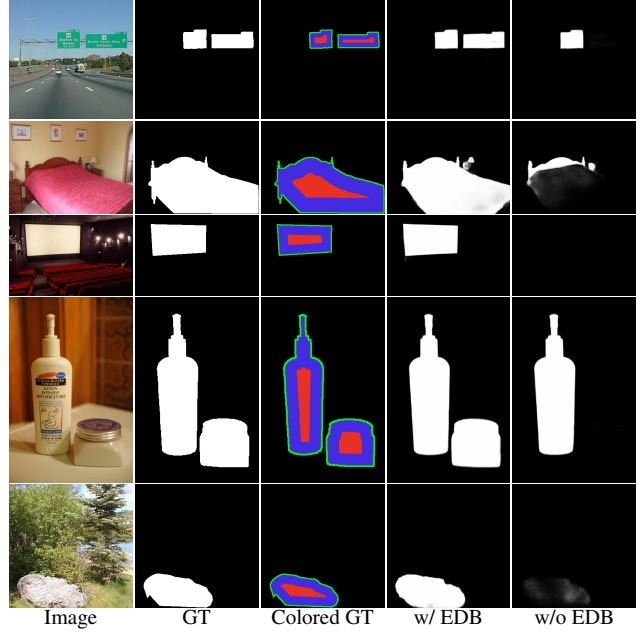


Figure 4. Visualization examples of our method with or without EDB. Red, green, and blue pixels in the colored ground-truth saliency map indicate the center, boundary and other pixels of salient objects, respectively. GT: Ground-truth

Setting	Type	ECSSD	DUTS-TE	DUT-O	HKU-IS	PASCAL-S
Baseline	Center	0.060	0.084	0.178	0.053	0.110
		0.046	0.062	0.124	0.043	0.082
		23.6%	26.6%	30.1%	19.3%	25.7%
+EDB	Boundary	0.223	0.243	0.335	0.202	0.262
		0.210	0.226	0.291	0.196	0.236
		6.1%	7.0%	13.0%	3.1%	10.2%
Rel. Impv.	Other	0.078	0.093	0.181	0.073	0.141
		0.062	0.076	0.133	0.065	0.112
		20.8%	18.1%	26.2%	11.5%	20.7%

Table 1. Evaluation of the baseline with or without EDB in terms of the MAE metric. “Rel. Impv.” indicates the relative improvement after applying extreme downsampling. DUT-O: DUT-OMRON

Δ MAE and MAE of the baseline, where Δ MAE is the decrease of MAE by adding EDB to the baseline. With applying EDB, we observe that the relative improvement in terms of center regions is much larger than that in terms of boundaries and other regions, which suggests that the improvement brought by EDB mainly comes from the accurate localization of salient objects. Fig. 1 shows that the accuracy of salient object localization has been saturated since 2019, while EDB boosts such accuracy significantly. Therefore, EDB has achieved its goal for improving SOD through better salient object localization. Moreover, it is interesting to find that EDB also has some improvement in terms of boundaries, although it is designed for high-level feature learning. Maybe this is because powerful high-level features make the decoding process easier, leading to better

Method	Speed (FPS)	#Param (M)	ECSSD [50]			DUTS-TE [39]			DUT-OMRON [51]			HKU-IS [18]			PASCAL-S [20]		
			F_β	F_β^w	MAE	F_β	F_β^w	MAE	F_β	F_β^w	MAE	F_β	F_β^w	MAE	F_β	F_β^w	MAE
VGG Backbone [36]																	
DHSNet [23]	10	94.04	0.903	0.837	0.062	0.807	0.705	0.066	-	-	-	0.889	0.816	0.053	0.820	0.731	0.092
ELD [16]	1.0	43.09	0.866	0.783	0.081	0.727	0.607	0.092	0.700	0.592	0.092	0.837	0.743	0.074	0.770	0.665	0.121
NLDF [26]	18.5	35.49	0.902	0.835	0.066	0.806	0.710	0.065	0.753	0.634	0.080	0.902	0.838	0.048	0.822	0.732	0.098
DSS [10]	7.0	62.23	0.905	0.832	0.065	0.813	0.700	0.065	0.760	0.643	0.074	0.900	0.821	0.050	0.829	0.742	0.095
Amulet [55]	9.7	33.15	0.913	0.839	0.061	0.778	0.657	0.085	0.743	0.626	0.098	0.897	0.817	0.051	0.807	0.707	0.109
UCF [56]	12	23.98	0.901	0.805	0.071	0.772	0.595	0.112	0.730	0.573	0.120	0.888	0.779	0.062	0.819	0.670	0.127
PiCANet [24]	5.6	32.85	0.923	0.862	0.049	0.837	0.745	0.054	0.766	0.691	0.068	0.916	0.847	0.042	0.852	0.767	0.078
C2S [19]	16.7	137.03	0.908	0.849	0.057	0.811	0.717	0.062	0.759	0.663	0.072	0.898	0.835	0.046	0.843	0.765	0.081
RAS [2]	20.4	20.13	0.917	0.855	0.058	0.831	0.739	0.059	0.785	0.695	0.063	0.914	0.849	0.045	0.828	0.735	0.100
PoolNet [22]	43.1	52.51	0.934	0.875	0.048	0.866	0.783	0.043	0.791	0.710	0.057	0.925	0.864	0.037	0.863	0.782	0.073
AFNet [5]	28.4	35.98	0.931	0.880	0.045	0.857	0.784	0.046	0.784	0.717	0.057	0.921	0.869	0.036	0.861	0.797	0.070
CPD [47]	68.0	29.23	0.932	0.889	0.043	0.864	0.799	0.043	0.794	0.715	0.057	0.924	0.879	0.033	0.861	0.796	0.072
EGNet [59]	10.7	108.07	0.938	0.886	0.044	0.871	0.796	0.044	0.794	0.728	0.056	0.928	0.875	0.034	0.856	0.788	0.077
GateNet [62]	-	-	0.933	0.881	0.045	0.866	0.785	0.045	0.784	0.703	0.061	0.927	0.872	0.036	0.868	0.797	0.068
ITSD [63]	53.0	17.08	0.933	0.888	0.044	0.875	0.813	0.042	0.802	0.734	0.063	0.926	0.881	0.035	0.869	0.811	0.068
MINet [30]	22.3	47.56	0.937	0.899	0.040	0.870	0.812	0.040	0.780	0.719	0.057	0.929	0.889	0.032	0.864	0.808	0.065
EDN (Ours)	43.7	21.83	0.943	0.908	0.038	0.881	0.822	0.041	0.805	0.746	0.057	0.938	0.900	0.029	0.875	0.815	0.066
ResNet Backbone [8]																	
SRM [40]	12.3	43.74	0.915	0.849	0.057	0.826	0.721	0.059	0.769	0.658	0.069	0.906	0.835	0.046	0.838	0.752	0.084
BRN [41]	3.6	126.35	0.920	0.887	0.043	0.827	0.774	0.050	0.774	0.709	0.062	0.910	0.875	0.036	0.849	0.795	0.072
CPD [47]	32.4	47.85	0.936	0.893	0.040	0.865	0.794	0.043	0.797	0.719	0.056	0.925	0.875	0.034	0.859	0.794	0.071
BASNet [32]	36.2	87.06	0.938	0.898	0.040	0.859	0.802	0.048	0.805	0.751	0.056	0.928	0.889	0.032	0.854	0.793	0.076
PoolNet [22]	40.5	68.26	0.938	0.889	0.042	0.874	0.806	0.040	0.792	0.729	0.055	0.930	0.881	0.033	0.862	0.793	0.075
EGNet [59]	9.9	111.69	0.940	0.897	0.041	0.878	0.814	0.039	0.792	0.738	0.053	0.932	0.886	0.031	0.862	0.795	0.074
GCPANet [3]	51.7	67.06	0.942	0.899	0.037	0.881	0.820	0.038	0.796	0.734	0.057	0.935	0.889	0.032	0.865	0.808	0.063
GateNet [62]	-	-	0.940	0.889	0.043	0.883	0.808	0.040	0.806	0.729	0.055	0.931	0.880	0.034	0.869	0.797	0.068
ITSD [63]	47.3	26.47	0.943	0.905	0.037	0.882	0.822	0.041	0.818	0.750	0.061	0.934	0.894	0.031	0.870	0.812	0.066
MINet [30]	31.1	162.38	0.942	0.906	0.037	0.880	0.824	0.038	0.795	0.738	0.056	0.934	0.897	0.029	0.865	0.809	0.064
EDN (Ours)	76.0	34.36	0.945	0.906	0.038	0.889	0.834	0.037	0.818	0.764	0.051	0.939	0.904	0.028	0.876	0.822	0.064

Table 2. Comparison of EDN with state-of-the-art SOD methods. The best performance in each column is highlighted in bold.

utilization of low-level features. Some visualization examples are provided in Fig. 4. EDB can help the system detect all salient objects. Without EDB, some salient objects will be lost completely (the 1st, 3rd, and 4th rows) or partially (the 2nd and 5th rows).

5. Experiments

5.1. Experimental Setup

Implementation details. The proposed method is implemented using the PyTorch library [31]. The training of all experiments is conducted using the Adam [15] optimizer with parameters $\beta_1 = 0.9$, $\beta_2 = 0.99$, weight decay 10^{-4} , and batch size 24. The backbone network of EDN is pretrained on ImageNet. The training lasts for 30 epochs in total. We adopt the *poly* learning rate scheduler so that the learning rate for the n^{th} epoch is $init_lr \times \left(1 - \frac{n}{max_epoch}\right)^{power}$, where we have $init_lr = 5 \times 10^{-5}$ and $power = 0.9$. In the training, we freeze the batch normalization layers of the backbone network as commonly used.

Datasets. We extensively evaluate the proposed EDN on five datasets, including DUTS [39], ECSSD [50], HKU-IS [18], PASCAL-S [20], and DUT-OMRON [51] datasets.

These five datasets consist of 15572, 1000, 4447, 850 and 5168 natural images with corresponding pixel-level labels. Following recent studies [24, 40, 41, 52], we train EDN on the DUTS training set and evaluate on the DUTS test set (DUTS-TE) and other four datasets.

Evaluation criteria. We evaluate EDN against previous state-of-the-art methods with regard to three widely-used metrics, *i.e.*, F-measure score (F_β), mean absolute error (MAE), and weighted F-measure score (F_β^w). For the first metric, F-measure is the weighted harmonic mean of precision and recall, like

$$F_\beta = \frac{(1 + \beta^2) \times \text{Precision} \times \text{Recall}}{\beta^2 \times \text{Precision} + \text{Recall}}, \quad (15)$$

where we set $\beta^2 = 0.3$ to emphasize the importance of precision, following previous works [10, 22, 24, 55]. Higher F-measure indicates better performance. The second metric, MAE, measures the similarity between the predicted saliency map P and the ground-truth saliency map G , which can be computed as

$$\text{MAE}(P, G) = \frac{1}{HW} \sum_{i=1}^H \sum_{j=1}^W |P_{i,j} - G_{i,j}|, \quad (16)$$

where H and W denote the height and width of the saliency map, respectively. The lower the MAE is, the better the

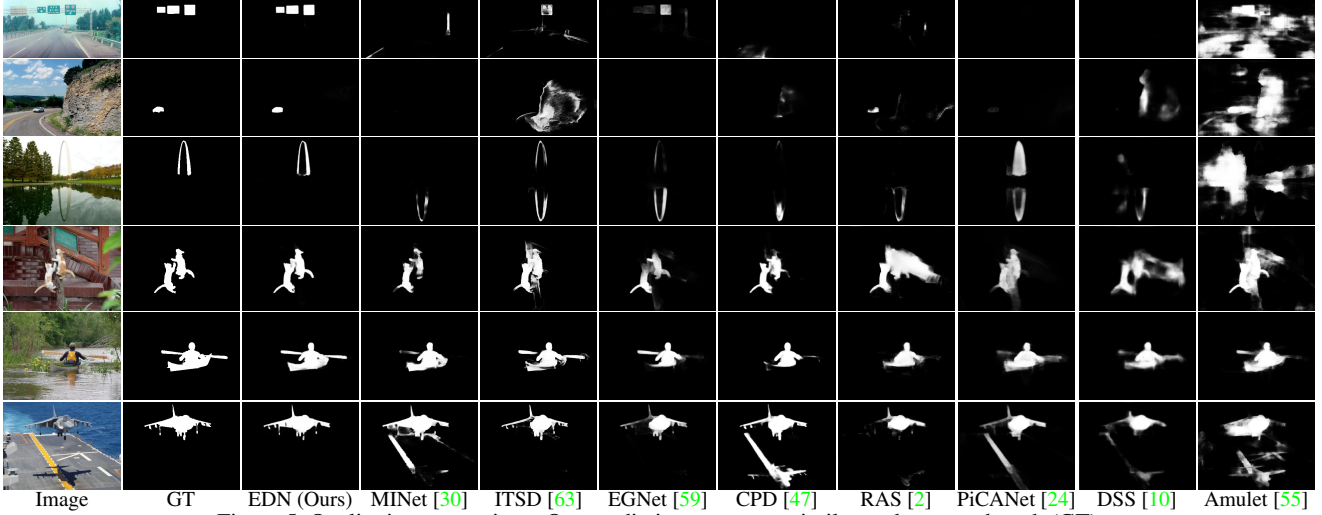


Figure 5. Qualitative comparison. Our predictions are more similar to the ground-truth (GT).

SOD method is. The third metric, weighted F-measure F_{β}^w , solves the problems of F-measure that may cause interpolation flaw, dependency flaw, and equal-importance flaw [28]. We use the official code with the default setting of the authors to conduct evaluation. The higher the weighted F-measure is, the better the performance is.

5.2. Comparison with State-of-the-art Methods

In this part, we compare the proposed EDN with existing 20 recent methods, including DHSNet [23], ELD [16], NLDF [26], DSS [10], Amulet [55], UCF [56], PiCANet [24], C2S [19], RAS [2], PoolNet [22], AFNet [5], CPD [47], EGNet [59], GateNet [62], ITSD [63], MINet [63], BRN [41], SRM [40], BASNet [32], and GCPANet [3]. We evaluate them using both VGG16 [36] and ResNet-50 [8] backbones. For a fair comparison, we use the saliency maps provided by them and if not provided, we directly use their official code and models to compute the missing saliency maps. We also report the speed and parameters of each method for reference. The speed is tested using a single NVIDIA TITAN Xp GPU.

Quantitative comparison. We show the results in Tab. 2. EDN consistently achieves the best performance in most cases, and in the remaining several cases, EDN is also very close to the best performance. EDN also has real-time speed and a relative small number of parameters. This demonstrates the efficacy and efficiency of EDN.

Qualitative comparison. The qualitative comparison is displayed in Fig. 5. While other competitors may not detect the whole salient objects or even not find some salient object in various scenarios, EDN can segment salient objects with clear boundaries.

5.3. Ablation Study

In this section, we conduct the ablation study for EDN equipped with the proposed EDB and SCPC. All experiments in this part are based on the VGG-16 backbone [36]. Other settings are the same as §5.1.

Effect of various design choices for EDB. Other than showing the effect of the whole EDB in §4, here we conduct analyses on the interior design choices of EDB. More specifically, we control the number of downsampling operations and the allowance of global attention to the output features in EDB. The results are summarized in Tab. 3. “Backbone” means to predict saliency maps directly from the last stage of the VGG16 backbone. “EDB (A)” indicates EDB only with one downsampling block, *i.e.*, “Down1” in Fig. 2. “EDB (B)” refers to EDB only with two downsampling blocks, *i.e.*, “Down1” and “Down2” in Fig. 2. “EDB (C)” only removes downsampling operations but remains all convolutions and global attention (Equ. (7) - Equ. (9)). We can see that “EDB (B)” outperforms “EDB (A)”, and both of them substantially outperforms “EDB (C)” and the baseline without EDB. This demonstrates the significance of downsampling and global attention in EDB, and removing each element will substantially affect the performance.

Comparison of EDB with other alternatives. Here, we replace EDB with other modules for high-level feature learning, like ASPP [1], PSP [57], and Non-local (NL) [44] modules. ASPP and PSP modules perform multi-scale feature learning using multiple separate branches. The results are shown in Tab. 5. We can find that adding ASPP, PSP, or NL module to the baseline only achieves slightly better or even worse performance. In contrast, EDB outperforms ASPP, PSP, NL, and the baseline by a large margin, demon-

No.	Method	ECSSD [50]			DUTS-TE [39]			DUT-OMRON [51]			HKU-IS [18]			PASCAL-S [20]		
		F_β	F_β^w	MAE	F_β	F_β^w	MAE	F_β	F_β^w	MAE	F_β	F_β^w	MAE	F_β	F_β^w	MAE
1	Backbone	0.883	0.812	0.071	0.779	0.691	0.065	0.682	0.573	0.094	0.883	0.819	0.049	0.814	0.733	0.091
2	No. 1+Decoder	0.933	0.896	0.041	0.871	0.816	0.039	0.780	0.725	0.054	0.932	0.896	0.030	0.864	0.806	0.068
3	No. 2+EDB (A)	0.938	0.905	0.038	0.874	0.820	0.041	0.794	0.741	0.056	0.934	0.899	0.029	0.871	0.818	0.064
4	No. 2+EDB (B)	0.939	0.904	0.039	0.876	0.822	0.041	0.803	0.747	0.056	0.936	0.901	0.029	0.873	0.819	0.066
5	No. 2+EDB (C)	0.937	0.900	0.039	0.861	0.797	0.047	0.798	0.728	0.062	0.931	0.893	0.031	0.865	0.805	0.068
6	No. 2+EDB	0.943	0.908	0.038	0.881	0.822	0.041	0.805	0.746	0.057	0.938	0.900	0.029	0.875	0.815	0.066

Table 3. Evaluation of various design choices of EDB.

No.	Setting	ECSSD [50]			DUTS-TE [39]			DUT-OMRON [51]			HKU-IS [18]			PASCAL-S [20]		
		L	H	EH	F_β	F_β^w	MAE	F_β	F_β^w	MAE	F_β	F_β^w	MAE	F_β	F_β^w	MAE
1	(b)	-	-	-	0.941	0.906	0.038	0.877	0.824	0.041	0.802	0.745	0.057	0.937	0.901	0.029
2	(c)	-	-	-	0.940	0.906	0.038	0.880	0.825	0.040	0.804	0.750	0.054	0.935	0.899	0.030
3	-	(a)	-	-	0.941	0.908	0.037	0.875	0.820	0.042	0.798	0.740	0.059	0.935	0.900	0.029
4	-	(c)	-	-	0.940	0.905	0.040	0.878	0.824	0.039	0.800	0.747	0.054	0.935	0.900	0.029
5	-	-	(a)	-	0.939	0.900	0.041	0.873	0.809	0.044	0.803	0.741	0.059	0.933	0.893	0.032
6	-	-	(b)	-	0.941	0.903	0.040	0.873	0.811	0.045	0.801	0.737	0.061	0.935	0.896	0.030
7	-	-	-	-	0.943	0.908	0.038	0.881	0.822	0.041	0.805	0.746	0.057	0.938	0.900	0.029

Table 4. Evaluation of various atrous rate settings for SCPC. The last row is the default setting.

Method	ECSSD [50]			PASCAL-S [20]		
	F_β	F_β^w	MAE	F_β	F_β^w	MAE
Baseline	0.933	0.896	0.041	0.864	0.806	0.068
+ASPP [1]	0.935	0.895	0.042	0.856	0.800	0.070
+PSP [57]	0.935	0.896	0.041	0.869	0.810	0.068
+NL [44]	0.932	0.895	0.041	0.870	0.809	0.068
+EDB	0.943	0.908	0.038	0.875	0.815	0.066

Table 5. Comparison of EDB with other alternatives. The baseline is EDN without EDB (No. 2 in Tab. 3).

strating the superiority of our extreme downsampling technique. Please refer to supplementary for complete results on five datasets.

Atrous rate configurations of SCPC. EDN has six downsampling operations, downsampling the feature map by half each time. Correspondingly, there are seven SCPC modules whose atrous rates are set according to the size of the feature map, as shown in Fig. 2. We show the results of different atrous rate settings for SCPC in Tab. 4. We divide our seven times of mutli-level feature fusion into 3 groups. “L” (low) includes the first two stages that output feature maps with the highest resolutions. “H” (high) includes the 3rd, 4th, and 5th stages. “EH” (extremely high) includes the last two extra scales of feature maps in EDB. For different groups, we apply different atrous rate settings. By default, the atrous rates of four branches in SCPC for the group “L”, “H”, and “EH” are set as {1,2,4,8} (a), {1,2,3,4} (b), and {1,1,1,1} (c), respectively. In Tab. 4, we tried other two types of atrous rate settings for each group. We can observe that the results only fluctuates slightly with various atrous rates, demonstrating that the proposed SCPC is robust for different atrous rate settings. Since the 7th setting in Tab. 4 achieves the overall best performance, we employ it as the default setting for SCPC.

Comparison of SCPC with other alternatives. In this part, we compare the proposed SCPC with the vanilla con-

Method	DUTS-TE [39]			DUT-OMRON [51]		
	F_β	F_β^w	MAE	F_β	F_β^w	MAE
Conv	0.837	0.776	0.048	0.740	0.662	0.070
ASPP	0.864	0.805	0.042	0.774	0.712	0.057
SCPC	0.871	0.816	0.039	0.780	0.725	0.054

Table 6. Ablation study for the proposed SCPC.

volution (“Conv”) and ASPP. Specifically, we first replace SCPC with 3 × 3 convolutions that have the same number of output channels as SCPC, resulting in a decoder similar to U-Net [34]. Then, we replace SCPC with ASPP by removing the scale correlation in SCPC, *i.e.*, removing the sum term of M_3^{i-1} in Equ. (13). The results are displayed in Tab. 6. We can see that ASPP outperforms “Conv” significantly, and SCPC further improves ASPP substantially, suggesting the effectiveness of SCPC in feature fusion.

6. Conclusion

Multi-scale learning is the core for SOD by leveraging high-level semantic features for salient object localization and low-level fine details for boundary discovering [2, 10, 24, 40–42, 52, 54, 55]. However, existing SOD methods mainly focus on learning/utilizing low-level features by designing various multi-level feature fusion strategies [2, 9, 12, 13, 21, 23, 24, 40, 42, 54, 55] or imposing boundary supervision directly [5, 19, 22, 32, 37, 43, 45, 46, 48, 59, 63], while leaving high-level feature learning less investigated. This paper suggests that we should put more efforts on high-level feature learning, whose discard has caused salient object localization saturated since 2019 (see Fig. 1). To this end, we propose an extremely-downsampled block (EDB) to learn a global view of the whole image, making salient object localization more accurate. We also propose a scale-correlated pyramid convolution (SCPC) to build an elegant and effective decoder to recover object details from the above extreme downsampling. This research is expected to spark some new thinking in SOD.

References

[1] Liang-Chieh Chen, George Papandreou, Iasonas Kokkinos, Kevin Murphy, and Alan L Yuille. Deeplab: Semantic image segmentation with deep convolutional nets, atrous convolution, and fully connected crfs. *IEEE TPAMI*, 40(4):834–848, 2017. [2](#), [3](#), [4](#), [7](#), [8](#)

[2] Shuhan Chen, Xiuli Tan, Ben Wang, and Xuelong Hu. Reverse attention for salient object detection. In *ECCV*, 2018. [1](#), [2](#), [3](#), [6](#), [7](#), [8](#)

[3] Zuyao Chen, Qianqian Xu, Runmin Cong, and Qingming Huang. Global context-aware progressive aggregation network for salient object detection. In *AAAI*, pages 10599–10606, 2020. [6](#), [7](#)

[4] Ming-Ming Cheng, Niloy J Mitra, Xiaolei Huang, Philip HS Torr, and Shi-Min Hu. Global contrast based salient region detection. *IEEE TPAMI*, 37(3):569–582, 2015. [1](#), [2](#)

[5] Mengyang Feng, Huchuan Lu, and Errui Ding. Attentive feedback network for boundary-aware salient object detection. In *IEEE CVPR*, pages 1623–1632, 2019. [1](#), [6](#), [7](#), [8](#)

[6] Yue Gao, Meng Wang, Zheng-Jun Zha, Jialie Shen, Xuelong Li, and Xindong Wu. Visual-textual joint relevance learning for tag-based social image search. *IEEE TIP*, 22(1):363–376, 2013. [1](#)

[7] Chen Gong, Dacheng Tao, Wei Liu, Stephen J Maybank, Meng Fang, Keren Fu, and Jie Yang. Saliency propagation from simple to difficult. In *IEEE CVPR*, pages 2531–2539, 2015. [2](#)

[8] Kaiming He, Xiangyu Zhang, Shaoqing Ren, and Jian Sun. Deep residual learning for image recognition. In *IEEE CVPR*, pages 770–778, 2016. [5](#), [6](#), [7](#)

[9] Shengfeng He, Jianbo Jiao, Xiaodan Zhang, Guoqiang Han, and Rynson WH Lau. Delving into salient object subitizing and detection. In *IEEE ICCV*, pages 1059–1067, 2017. [1](#), [2](#), [3](#), [8](#)

[10] Qibin Hou, Ming-Ming Cheng, Xiaowei Hu, Ali Borji, Zhiwen Tu, and Philip Torr. Deeply supervised salient object detection with short connections. *IEEE TPAMI*, 41(4):815–828, 2019. [1](#), [2](#), [6](#), [7](#), [8](#)

[11] Zilong Huang, Xinggang Wang, Lichao Huang, Chang Huang, Yunchao Wei, and Wenyu Liu. CCNet: Criss-cross attention for semantic segmentation. In *IEEE ICCV*, pages 603–612, 2019. [2](#)

[12] Md Amirul Islam, Mahmoud Kalash, and Neil DB Bruce. Revisiting salient object detection: Simultaneous detection, ranking, and subitizing of multiple salient objects. In *IEEE CVPR*, pages 7142–7150, 2018. [1](#), [2](#), [3](#), [8](#)

[13] Sen Jia and Neil DB Bruce. Richer and deeper supervision network for salient object detection. *arXiv preprint arXiv:1901.02425*, 2019. [1](#), [2](#), [3](#), [8](#)

[14] Huaizu Jiang, Jingdong Wang, Zejian Yuan, Yang Wu, Nanning Zheng, and Shipeng Li. Salient object detection: A discriminative regional feature integration approach. In *IEEE CVPR*, pages 2083–2090, 2013. [1](#), [2](#)

[15] Diederik Kingma and Jimmy Ba. Adam: A method for stochastic optimization. In *ICLR*, 2015. [6](#)

[16] Gayoung Lee, Yu-Wing Tai, and Junmo Kim. Deep saliency with encoded low level distance map and high level features. In *IEEE CVPR*, pages 660–668, 2016. [1](#), [2](#), [6](#), [7](#)

[17] Guanbin Li, Yuan Xie, Liang Lin, and Yizhou Yu. Instance-level salient object segmentation. In *IEEE CVPR*, pages 247–256, 2017. [1](#)

[18] Guanbin Li and Yizhou Yu. Visual saliency based on multi-scale deep features. In *IEEE CVPR*, pages 5455–5463, 2015. [2](#), [6](#), [8](#)

[19] Xin Li, Fan Yang, Hong Cheng, Wei Liu, and Dinggang Shen. Contour knowledge transfer for salient object detection. In *ECCV*, pages 355–370, 2018. [1](#), [6](#), [7](#), [8](#)

[20] Yin Li, Xiaodi Hou, Christof Koch, James M Rehg, and Alan L Yuille. The secrets of salient object segmentation. In *IEEE CVPR*, pages 280–287, 2014. [6](#), [8](#)

[21] Zun Li, Congyan Lang, Yunpeng Chen, Junhao Liew, and Jiashi Feng. Deep reasoning with multi-scale context for salient object detection. *arXiv preprint arXiv:1901.08362*, 2019. [1](#), [2](#), [3](#), [8](#)

[22] Jiang-Jiang Liu, Qibin Hou, Ming-Ming Cheng, Jiashi Feng, and Jianmin Jiang. A simple pooling-based design for real-time salient object detection. In *IEEE CVPR*, pages 3917–3926, 2019. [1](#), [2](#), [3](#), [6](#), [7](#), [8](#)

[23] Nian Liu and Junwei Han. DHSNet: Deep hierarchical saliency network for salient object detection. In *IEEE CVPR*, pages 678–686, 2016. [1](#), [2](#), [6](#), [7](#), [8](#)

[24] Nian Liu, Junwei Han, and Ming-Hsuan Yang. Picanet: Pixel-wise contextual attention learning for accurate saliency detection. *IEEE TIP*, 2020. [1](#), [2](#), [3](#), [6](#), [7](#), [8](#)

[25] Yun Liu, Yu-Huan Wu, Pei-Song Wen, Yu-Jun Shi, Yu Qiu, and Ming-Ming Cheng. Leveraging instance-, image- and dataset-level information for weakly supervised instance segmentation. *IEEE TPAMI*, 2020. [1](#)

[26] Zhiming Luo, Akshaya Kumar Mishra, Andrew Achkar, Justin A Eichel, Shaozi Li, and Pierre-Marc Jodoin. Non-local deep features for salient object detection. In *IEEE CVPR*, pages 6609–6617, 2017. [1](#), [6](#), [7](#)

[27] Vijay Mahadevan and Nuno Vasconcelos. Saliency-based discriminant tracking. In *IEEE CVPR*, 2009. [1](#)

[28] Ran Margolin, Lihi Zelnik-Manor, and Ayallet Tal. How to evaluate foreground maps? In *IEEE CVPR*, pages 248–255, 2014. [7](#)

[29] Fausto Milletari, Nassir Navab, and Seyed-Ahmad Ahmadi. V-Net: Fully convolutional neural networks for volumetric medical image segmentation. In *International Conference on 3D Vision*, pages 565–571. IEEE, 2016. [4](#)

[30] Youwei Pang, Xiaoqi Zhao, Lihe Zhang, and Huchuan Lu. Multi-scale interactive network for salient object detection. In *IEEE CVPR*, pages 9413–9422, 2020. [1](#), [6](#), [7](#)

[31] Adam Paszke, Sam Gross, Soumith Chintala, Gregory Chanan, Edward Yang, Zachary DeVito, Zeming Lin, Alban Desmaison, Luca Antiga, and Adam Lerer. Automatic differentiation in PyTorch. In *NIPS Workshop*, 2017. [6](#)

[32] Xuebin Qin, Zichen Zhang, Chenyang Huang, Chao Gao, Masood Dehghan, and Martin Jagersand. BASNet: Boundary-aware salient object detection. In *IEEE CVPR*, pages 7479–7489, 2019. [1](#), [6](#), [7](#), [8](#)

[33] Zhixiang Ren, Shenghua Gao, Liang-Tien Chia, and Ivor Wai-Hung Tsang. Region-based saliency detection and its application in object recognition. *IEEE TCSVT*, 24(5):769–779, 2014. 1

[34] Olaf Ronneberger, Philipp Fischer, and Thomas Brox. U-Net: Convolutional networks for biomedical image segmentation. In *MICCAI*, pages 234–241, 2015. 1, 8

[35] Evan Shelhamer, Jonathan Long, and Trevor Darrell. Fully convolutional networks for semantic segmentation. *IEEE TPAMI*, 39(4):640, 2017. 2, 3

[36] Karen Simonyan and Andrew Zisserman. Very deep convolutional networks for large-scale image recognition. In *ICLR*, 2015. 3, 6, 7

[37] Jinning Su, Jia Li, Yu Zhang, Changqun Xia, and Yonghong Tian. Selectivity or invariance: Boundary-aware salient object detection. In *IEEE ICCV*, pages 3799–3808, 2019. 1, 2, 8

[38] Wei-Chih Tu, Shengfeng He, Qingxiong Yang, and Shao-Yi Chien. Real-time salient object detection with a minimum spanning tree. In *IEEE CVPR*, pages 2334–2342, 2016. 2

[39] Lijun Wang, Huchuan Lu, Yifan Wang, Mengyang Feng, Dong Wang, Baocai Yin, and Xiang Ruan. Learning to detect salient objects with image-level supervision. In *IEEE CVPR*, pages 136–145, 2017. 6, 8

[40] Tiantian Wang, Ali Borji, Lihe Zhang, Pingping Zhang, and Huchuan Lu. A stagewise refinement model for detecting salient objects in images. In *IEEE ICCV*, pages 4019–4028, 2017. 1, 2, 3, 6, 7, 8

[41] Tiantian Wang, Lihe Zhang, Shuo Wang, Huchuan Lu, Gang Yang, Xiang Ruan, and Ali Borji. Detect globally, refine locally: A novel approach to saliency detection. In *IEEE CVPR*, pages 3127–3135, 2018. 1, 6, 7, 8

[42] Wenguan Wang, Jianbing Shen, Xingping Dong, and Ali Borji. Salient object detection driven by fixation prediction. In *IEEE CVPR*, pages 1711–1720, 2018. 1, 2, 3, 8

[43] Wenguan Wang, Shuyang Zhao, Jianbing Shen, Steven CH Hoi, and Ali Borji. Salient object detection with pyramid attention and salient edges. In *IEEE CVPR*, pages 1448–1457, 2019. 1, 8

[44] Xiaolong Wang, Ross Girshick, Abhinav Gupta, and Kaiming He. Non-local neural networks. In *IEEE CVPR*, pages 7794–7803, 2018. 7, 8

[45] Xiang Wang, Huimin Ma, Xiaozhi Chen, and Shaodi You. Edge preserving and multi-scale contextual neural network for salient object detection. *IEEE TIP*, 27(1):121–134, 2017. 1, 8

[46] Yupei Wang, Xin Zhao, Xuecai Hu, Yin Li, and Kaiqi Huang. Focal boundary guided salient object detection. *IEEE TIP*, 28(6):2813–2824, 2019. 1, 8

[47] Zhe Wu, Li Su, and Qingming Huang. Cascaded partial decoder for fast and accurate salient object detection. In *IEEE CVPR*, pages 3907–3916, 2019. 6, 7

[48] Zhe Wu, Li Su, and Qingming Huang. Stacked cross refinement network for edge-aware salient object detection. In *IEEE ICCV*, pages 7264–7273, 2019. 1, 8

[49] Changqun Xia, Jia Li, Xiaowu Chen, Anlin Zheng, and Yu Zhang. What is and what is not a salient object? Learning salient object detector by ensembling linear exemplar regressors. In *IEEE CVPR*, pages 4321–4329, 2017. 2

[50] Qiong Yan, Li Xu, Jianping Shi, and Jiaya Jia. Hierarchical saliency detection. In *IEEE CVPR*, pages 1155–1162, 2013. 6, 8

[51] Chuan Yang, Lihe Zhang, Huchuan Lu, Xiang Ruan, and Ming-Hsuan Yang. Saliency detection via graph-based manifold ranking. In *IEEE CVPR*, pages 3166–3173, 2013. 2, 6, 8

[52] Yu Zeng, Huchuan Lu, Lihe Zhang, Mengyang Feng, and Ali Borji. Learning to promote saliency detectors. In *IEEE CVPR*, pages 1644–1653, 2018. 1, 2, 6, 8

[53] Yi Zeng, Pingping Zhang, Jianming Zhang, Zhe Lin, and Huchuan Lu. Towards high-resolution salient object detection. In *IEEE ICCV*, pages 7234–7243, 2019. 2, 3

[54] Lu Zhang, Ju Dai, Huchuan Lu, You He, and Gang Wang. A bi-directional message passing model for salient object detection. In *IEEE CVPR*, pages 1741–1750, 2018. 1, 2, 3, 8

[55] Pingping Zhang, Dong Wang, Huchuan Lu, Hongyu Wang, and Xiang Ruan. Amulet: Aggregating multi-level convolutional features for salient object detection. In *IEEE ICCV*, pages 202–211, 2017. 1, 2, 3, 6, 7, 8

[56] Pingping Zhang, Dong Wang, Huchuan Lu, Hongyu Wang, and Baocai Yin. Learning uncertain convolutional features for accurate saliency detection. In *IEEE ICCV*, pages 212–221, 2017. 6, 7

[57] Hengshuang Zhao, Jianping Shi, Xiaojuan Qi, Xiaogang Wang, and Jiaya Jia. Pyramid scene parsing network. In *IEEE CVPR*, pages 2881–2890, 2017. 2, 3, 4, 7, 8

[58] Jia-Xing Zhao, Yang Cao, Deng-Ping Fan, Ming-Ming Cheng, Xuan-Yi Li, and Le Zhang. Contrast prior and fluid pyramid integration for rgbd salient object detection. In *IEEE CVPR*, 2019. 2

[59] Jia-Xing Zhao, Jiangjiang Liu, Den-Ping Fan, Yang Cao, Jufeng Yang, and Ming-Ming Cheng. EGNet: Edge guidance network for salient object detection. In *IEEE ICCV*, pages 8779–8788, 2019. 1, 3, 6, 7, 8

[60] Rui Zhao, Wanli Ouyang, Hongsheng Li, and Xiaogang Wang. Saliency detection by multi-context deep learning. In *IEEE CVPR*, pages 1265–1274, 2015. 2

[61] Ting Zhao and Xiangqian Wu. Pyramid feature attention network for saliency detection. In *IEEE CVPR*, pages 3085–3094, 2019. 2, 3

[62] Xiaoqi Zhao, Youwei Pang, Lihe Zhang, Huchuan Lu, and Lei Zhang. Suppress and balance: A simple gated network for salient object detection. In *ECCV*, 2020. 1, 6, 7

[63] Huajun Zhou, Xiaohua Xie, Jian-Huang Lai, Zixuan Chen, and Lingxiao Yang. Interactive two-stream decoder for accurate and fast saliency detection. In *IEEE CVPR*, pages 9141–9150, 2020. 1, 3, 6, 7, 8

[64] Zhen Zhu, Mengde Xu, Song Bai, Tengteng Huang, and Xiang Bai. Asymmetric non-local neural networks for semantic segmentation. In *IEEE ICCV*, pages 593–602, 2019. 2